Fast chemical reaction and multiple-scale concentration fields in singular vortices

D. Martinand* and J. C. Vassilicos
Turbulence and Mixing Group, Department of Aeronautics, Imperial College London, London SW7 2AZ, United Kingdom
(Received 9 October 2006; published 28 March 2007)

Two species involved in a simple, fast reaction tend to become segregated in patches composed of a single of these reactants. These patches are separated by a boundary where the stoichiometric condition is satisfied and the reaction occurs, fed by diffusion. Stirred by advection, this boundary and the concentration fields within the patches may tend to present multiple-scale characteristics. Based on this segregated state, this paper aims at evaluating the temporal evolutions of the length of the boundary and diffusive flux of reactants across it, when concentrations presenting initial self-similar fluctuations are advected by a singular vortex. First the two sources of singularity, i.e., the self-similar initial conditions and the singular vortex, are considered isolatedly. On the one hand, self-similar initial conditions are imposed to a diffusion-reaction system, for one- and two-dimensional cases. On the other hand, an imposed singular vortex advects initially on/off concentration fields, in combination with diffusion and reaction. This problem is addressed analytically, by characterizing the boundary by a box-counting dimension and the concentration fields by a Hölder exponent, and numerically, by direct numerical simulations of the advection-diffusion-reaction equations. Second, the way the two sources hang together shows that, depending on the self-similar properties of the initial concentration fields, the vortex promotes the chemical activity close to its inner smoothed-out core or close to the outer region where the boundary starts to spiral. For all the considered situations, the length of the boundary and the global reaction speed are found to evolve algebraically with time after a short transient and a good agreement is found between the analytical and numerical scaling laws.

DOI: 10.1103/PhysRevE.75.036315 PACS number(s): 47.70.Fw, 82.40.Ck, 47.32.−y

I. INTRODUCTION

The concentration field $c(\boldsymbol{x},t)$ of a reactant subjected to advection, diffusion, and reaction satisfies the equation

$$\partial_t c = -\mathbf{u}\cdot\boldsymbol{\nabla} c + \kappa\nabla^2 c - \upsilon, \tag{1}$$

where $\mathbf{u}$ is the velocity field, κ the diffusivity of the reactant, and υ the reaction term, a function of the concentration fields of the different reactants via the reaction kinetic. Of practical interest is the global reaction speed, noted V hereinafter, i.e., the reaction term integrated over the material domain. Considering initially nonpremixed reactants, with concentration fields presenting spatial fluctuations, fast diffusive and advective transports will mix the reactants before the reaction noticeably occurs. As far as V is concerned, the behavior of a perfectly mixed situation is recovered. On the contrary, slow transport mechanisms, considered in the forthcoming, are expected to abate the reaction by preventing the reactants to be set in contact. In this case, the importance of the spatial fluctuations of concentrations on the yield of the reaction has been acknowledged in various fields: chemical reactors (see, for instance, [1–3] and references therein) or atmospheric flows (where it is believed, for instance, to strongly influence the mechanisms of stratospheric ozone depletion [4–6]). In the first two situations, existing laminar or turbulent flows advecting the species obviously interact with the spatiotemporal fluctuations of concentrations.

The present paper is restricted to the case of a reaction between two reactants $A+B\rightarrow\Sigma P$, where P stands for product of the reaction. It leads to the reaction term $\upsilon=\gamma ab$ for a simple second order reaction, with a and b the concentrations in A and B and γ the kinetic constant of the reaction. Such a second order, collisional, reaction already presents a basic mechanism sustaining spatial fluctuations of concentrations and affecting V. The evolution of the concentrations under the sole effect of the reaction

$$d_t a = -\gamma ab,$$

$$d_t b = -\gamma ab, \tag{2}$$

is governed by the local initial values a_0 and b_0 of the concentrations. For $a_0\neq b_0$, the concentrations asymptotically decay exponentially [as $\exp(-\gamma|a_0-b_0|t)$] towards the equilibrium state $a_{\mathrm{eq}}=a_0-\min(a_0,b_0)$ and $b_{\mathrm{eq}}=b_0-\min(a_0,b_0)$. For $a_0=b_0$, the concentrations asymptotically decay algebraically (as t^{-1}) towards the equilibrium state $a_{\mathrm{eq}}=b_{\mathrm{eq}}=0$. Initial concentration fields presenting spatial fluctuations evolve towards the coexistence of patches, where the reactant originally locally in default is almost completely depleted and the reactant originally locally in excess remains. These patches are separated by a boundary, namely the set of points where the reactants are in their stoichiometric ratio ($a=b$). This boundary will be noted and referred to as $\mathcal{B}$ hereinafter. For one-, two-, and three-dimensional systems, $\mathcal{B}$ is, respectively, a set of disjoint points, curves, and surfaces.

Adding now slow diffusive transport to reaction, the patches behave as "tanks," feeding the reaction by diffusion of reactants towards $\mathcal{B}$. Owing to diffusion, reaction is expected to mostly occur in a band centered on $\mathcal{B}$. The geom-

*Present address: Laboratoire de Physique UMR CNRS 5672, École Normale Supérieure de Lyon, F-69364 Lyon Cedex 07, France.

etry and characteristic sizes of the patches of reactants and of $\mathcal{B}$ are governed by the fluctuations of the concentration fields down to the diffusive scale and are then expected to evolve with time.

This behavior has long been recognized and studied analytically and numerically in "discrete" systems of reaction-diffusion, i.e., where the particles of reactants exhibit a d-dimensional random walk. Within this framework, random initial fluctuations of the densities of particles lead to the breakup of the mean-field theory behind Eq. (2) for $d \leqslant 2$ and to the asymptotic behavior $V \propto t^{-1-d/4}$ for $d \leqslant 4$, numerically retrieved by Monte Carlo simulations [7–14]. In the forthcoming, a "mean-field" approach, where the reactants are described by concentration fields satisfying Eq. (1), is adopted exclusively, as this study focuses on the effect of fluctuations of these fields eventually advected by fluid flows. The relation between the "discrete" and "mean-field" approaches is then beyond the scope of this paper. It should also be kept in mind that the situations addressed here are one- and two-dimensional in the sense of three-dimensional systems presenting two or one invariant direction(s).

In cases where the Péclet number, i.e., the ratio between the characteristic times of diffusion and advection in Eq. (1), is large, the discrepancy between the size of the system and the diffusive scale induces high computational costs. Advected scalars are known to exhibit multiscale characteristics and continuous spectra in cases of turbulent [15], chaotic [16], and vortical [17] flows. It is then worthwhile to assess by analytical means, in simple generic cases, the quantitative effects of multiscale fluctuations of the concentration fields on V.

The present study aims at evaluating the scaling laws for V as a function of time for vortices advecting initially fluctuating concentration fields in two-dimensional situations. Coupling vortical flows and singular concentrations fields is of dual interest. Owing to the large values of the Schmidt number ν/κ usually observed in natural systems, where ν is the kinematic viscosity, the diffusive scale of the velocity field is larger than the diffusive scale of the concentration fields. A range of length scales where the variations of the velocity field are regular whereas the variations of the concentration fields are singular (the Batchelor regime) exists. A vortical flow constitutes an example of regular shear flow known to generate singularities in an advected scalar field. These singularities are related to the algebraic decay of the velocity field with the distance to the center of the vortex. They affect the large scale diffusive properties [17–22] and, consequently, the average reaction rate if fast reaction occurs in the system, as studied analytically [23,24] and observed experimentally [25]. These vortices can then be conceived of as an elementary ingredient of turbulent flows [26–28]. On another scale, large vortices are often encountered in geophysical flows, for instance, where these coherent structures advect fluctuating scalar fields, the singularity of which stems from the underlying turbulent velocity field. The Obukhov-Corrsin regime expected in the homogeneous and isotropic turbulent advection of a passive scalar is then known to be strongly dependent on large scale shear [29].

Analytically, the simplest framework to quantify the singularities of $\mathcal{B}$ and of the concentration fields is to assume a self-similar behavior. The boundary $\mathcal{B}$ is characterized by a box-counting dimension $D_{\mathcal{B}}$, such that the number of squares of edge ε required to cover this set is approximated over a range of ε's by the scaling law $N(\varepsilon) \sim (\varepsilon/\Lambda)^{-D_{\mathcal{B}}}$, where Λ is the integral scale of the set. Moreover, concentration fields such as their increments scale algebraically as $\overline{|c(\boldsymbol{x}+\boldsymbol{\varepsilon})-c(\boldsymbol{x})|} \propto |\boldsymbol{\varepsilon}|^h$ for small ε's are characterized by the Hölder exponent h. It is not elaborated much further here on the spatial- or ensemble-nature of the average (noted with an overbar).

Many previous analytical and numerical studies have focused on chaotic advection, seen as straining flow, coupled with diffusion for a passive scalar [30–33] or for autocatalytic [34,35] or more complex [36] reactions. On experimental and practical points of view, the case of a simple, collisional reaction, though more rarely tackled analytically in the presence of a flow, remains the most commonly encountered [37]. The behavior of diffusing scalars or reactants in straining flows remains a debated question between local and global interpretations [38,39]. As far as shear flows are concerned, their coupling with reaction has been often passed up as they do not constitute the most effective way to mix. Besides the interest of shear flows on their own, it should also be noted that they may be involved in the case of chaotic advection in a closed domain, in which surfaces where the trajectories of the fluid particles are integrable (KAM surfaces) are possible. The fluid particles remain attracted to these surfaces and the flow therein is a shear flow, which tends to govern the asymptotic mixing properties (see, for instance, [40]). Previous analytical and numerical studies have also focused on the coupling between a vortex and flames in premixed combustion, where pockets of unburned fuel are known to form and slow down the reaction [41,42]. The collisional reaction does not exhibit such a behavior as it is explained by the move of the reaction fronts relative to the fluid and is specific to premixed combustion.

Further assumptions are made throughout this paper. First, the reactants and the reaction are assumed not to retroact on the velocity field. Consequently, the velocity field will be considered as externally imposed. As this paper does not focus on the dynamics of these vortical structures but on their kinematic effects on scalar fields, its scope is restricted to the generic situation of two-dimensional vortices. Then, the reactants are assumed to present the same diffusivity κ.

Introducing the characteristic scales C for concentrations, L for lengths, and U for velocities, Eq. (1) is nondimensionalized using the characteristic time of reaction $(\gamma C)^{-1}$ and recast in the form

$$\partial_t a = -(1/\mathrm{Da})\mathbf{u}\cdot\boldsymbol{\nabla} a + (1/\mathrm{DaPe})\nabla^2 a - ab,$$

$$\partial_t b = -(1/\mathrm{Da})\mathbf{u}\cdot\boldsymbol{\nabla} b + (1/\mathrm{DaPe})\nabla^2 b - ab, \qquad (3)$$

with $\mathrm{Da} = \gamma CL/U$ the Damköhler number and $\mathrm{Pe} = UL/\kappa$ the Péclet number. To insist on the nature of rescaled diffusivity of this latter, $\mathcal{D}$ instead of 1/DaPe is used in the forthcoming.

The material is organized as follows: Sec. II is devoted to diffusion-reaction, with self-similarity governed by the initial conditions. In Sec. III, the self-similarity in a two-dimensional advection-diffusion-reaction system stems from

shear flows in the form of singular vortices acting on regular concentration fields. Section IV then combines the two sources of self-similarity. Finally, the results obtained are discussed in Sec. V.

II. DIFFUSION-REACTION OF INITIALLY SELF-SIMILAR CONCENTRATION FIELDS

We focus in this part on pure diffusion-reaction, i.e., on the solutions of

$$\partial_t a = \mathcal{D}\nabla^2 a - ab,$$

$$\partial_t b = \mathcal{D}\nabla^2 b - ab. \tag{4}$$

The multiscale behavior of the concentration fields is obtained by prescribing self-similar initial conditions. The basic mechanisms and results are first introduced for one-dimensional systems and the validity of their extension to two-dimensional situations is then established.

A. Orders of magnitude for quantities associated with $\mathcal{B}$

First, two A-rich and B-rich contiguous one-dimensional patches of characteristic length L and concentration C are considered. Owing to diffusion, the reaction tends to occur in a band centered on $\mathcal{B}$. The consumption of the reactants diffusing from the patches towards the band defines the characteristics of the band. In terms of order of magnitude, this band is characterized by a concentration $c_\mathcal{B}$, similar for A and B, and a width $s_\mathcal{B}$, as sketched in Fig. 1(a). These orders of magnitude result from two distinct mechanisms. First, as long as the characteristic diffusive length scale $\sqrt{\mathcal{D}t}$ remains smaller than the size of the patch L, the balance between diffusion from the patch and reaction integrated across the reactive band leads to

$$\mathcal{D}\frac{C}{\sqrt{\mathcal{D}t}} \sim c_\mathcal{B}^2 s_\mathcal{B}. \tag{5}$$

Second, within the reactive band, the balance between the characteristic times of diffusion and chemical reaction leads to

$$\frac{s_\mathcal{B}^2}{\mathcal{D}} \sim \frac{1}{c_\mathcal{B}}. \tag{6}$$

Equations (5) and (6) yield

$$s_\mathcal{B} \sim \left(\frac{\mathcal{D}\sqrt{\mathcal{D}t}}{C}\right)^{1/3} \tag{7}$$

and

$$c_\mathcal{B} \sim \left(\frac{\mathcal{D}C^2}{\sqrt{\mathcal{D}t}}\right)^{2/3}. \tag{8}$$

Equation (8) implies that the characteristic reaction term in the reactive band scales as

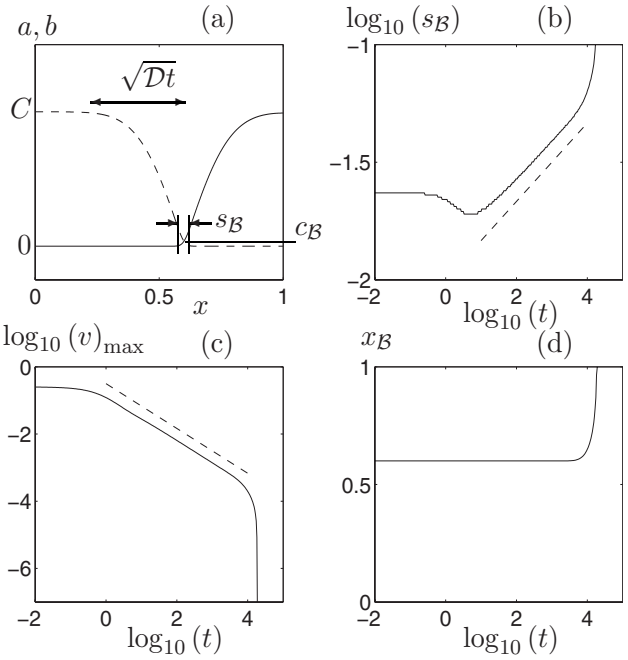

FIG. 1. One-dimensional numerical integration of Eq. (4) for an isolated $\mathcal{B}$, with $\mathcal{D}=10^{-5}$. (a) Concentration fields a (—) and b (—) at $t=1000$. (b) Numerically obtained temporal evolution of the width of the boundary (—), evaluated as the length of the domain where $0.1<a(x,t)/b(x,t)<10$, compared with the expected scaling law Eq. (7) (—). (c) Numerically obtained temporal evolution of the local maximum of the reaction term (—), compared with the expected scaling law Eq. (9) (—). (d) Numerically obtained temporal evolution of $x_\mathcal{B}$, the localization of $\mathcal{B}$.

$$v_\mathcal{B} = c_\mathcal{B}^2 \sim \left(\frac{\mathcal{D}C^2}{\sqrt{\mathcal{D}t}}\right)^{4/3}. \tag{9}$$

These scaling laws are compared with the results of a one-dimensional numerical simulation of Eq. (4) for on/off concentration fields presenting a single boundary point as depicted in Fig. 1(a). Due to its numerical stiffness, Eq. (4) is solved using the MATLAB partial differential equation solver, built on a variable order solver. The concentration fields are discretized on 2048 points. Vanishing Neumann boundary conditions are applied at $x=0$ and 1. The time dependencies of Eqs. (7) and (9) are favorably compared with the results of the numerical simulation in Figs. 1(b) and 1(c). It is also seen in Fig. 1(c) that the reaction speed decreases dramatically after diffusion has affected the whole rightward patch ($t>10\,000$). Indeed, as the characteristic diffusion length scale $\sqrt{\mathcal{D}t}$ reaches L, the concentration in the patch decays exponentially with characteristic time $L^2/\mathcal{D}$.

The width $s_\mathcal{B}$ in Eq. (7) increases with time less rapidly than $\sqrt{\mathcal{D}t}$ while $c_\mathcal{B}$ in Eq. (8) decreases with time. Thus in the limit of small $\mathcal{D}$'s (or fast reaction), the reactive band can be considered as infinitely thin, reduced to $\mathcal{B}$. Furthermore, the concentrations of both reactants tend to vanish on $\mathcal{B}$. Finally, it is also assumed in the forthcoming that the displacement of $\mathcal{B}$ is negligible. Indeed, the displacement of $\mathcal{B}$ observed in the numerical simulation of Fig. 1(d) appears to be negligible

before the collapse of the rightward patch. This displacement stems from the constraint that the diffusive fluxes on both sides of $\mathcal{B}$ have to be equal to satisfy the reaction stoichiometry. This last assumption is rather crude as in the case of multiscale concentration fields, discrepancies between diffusive fluxes on both side of $\mathcal{B}$ can be large for specific realizations.

Analytically, the idea is then to consider the solution $f=a-b$ of $\partial_t f=\mathcal{D}\nabla^2 f$, together with vanishing boundary conditions on $\mathcal{B}$. The concentration fields a and b are retrieved as $a=f$, $b=0$ for $f>0$ and $a=0$, $b=f$ for $f<0$. The global reaction speed then resumes to the diffusive flux across $\mathcal{B}$: $V=\int v dx=\mathcal{D}\Sigma_{\mathcal{B}}|\partial_x f|$, for a one-dimensional system.

B. One-dimensional self-similar case

A set of alternatively A-rich and B-rich one-dimensional patches is now considered. The initial set of points $\mathcal{B}$ between these patches is assumed to exhibit a box-counting dimension $D_{\mathcal{B}}$ and the initial concentration fields $a_0(x)$ and $b_0(x)$ a common Hölder exponent h. Within a patch, the concentration evolves under the action of diffusion and vanishes at the two consecutive points of $\mathcal{B}$ bordering the patch. A patch collapses when the diffusive length scale reaches its size. The dominant contributions to V are then due to patches larger than $\sqrt{\mathcal{D}t}$. Owing to its self-similarity, the number of points of $\mathcal{B}$ evolves as

$$N_{\mathcal{B}} \propto (\sqrt{\mathcal{D}t})^{-D_{\mathcal{B}}}. \tag{10}$$

The diffusive flux of the reactants through a point of $\mathcal{B}$ is then evaluated as follows, assuming that this point is located at $x_{\mathcal{B}}=0$ for the sake of simplicity. The field $f(x,t)$ vanishing at $x_{\mathcal{B}}$ and diffusing from the initial condition $f_0(x)$ evolves as

$$f(x,t)=\frac{1}{\sqrt{\pi}}\times\left(\int_{-x/\sqrt{4\mathcal{D}t}}^{\infty} f_0(u\sqrt{4\mathcal{D}t}+x)\exp(-u^2)du - \int_{x/\sqrt{4\mathcal{D}t}}^{\infty} f_0(u\sqrt{4\mathcal{D}t}-x)\exp(-u^2)du\right). \tag{11}$$

For $f_0(x)$ presenting a Hölder exponent h and vanishing at $x=0$, the statistical average of f at time t reads

$$\overline{|f(x,t)|}\propto\frac{1}{\sqrt{\pi}}\times\left(\int_{-x/\sqrt{4\mathcal{D}t}}^{\infty}(u\sqrt{4\mathcal{D}t}+x)^h\exp(-u^2)du - \int_{x/\sqrt{4\mathcal{D}t}}^{\infty}(u\sqrt{4\mathcal{D}t}-x)^h\exp(-u^2)du\right). \tag{12}$$

The average of the flux at $x_{\mathcal{B}}$ then reads

$$\mathcal{D}\overline{|\partial_x f(0,t)|}\propto\frac{2\mathcal{D}}{\sqrt{\pi}}\left(\int_0^{\infty}(u\sqrt{4\mathcal{D}t})^{h-1}\exp(-u^2)du\right) \propto\mathcal{D}\frac{2h}{\sqrt{\pi}}\Gamma\left(\frac{h}{2}\right)(\sqrt{4\mathcal{D}t})^{h-1}, \tag{13}$$

where Γ is the gamma function. The global reaction speed then scales algebraically with $\mathcal{D}$ and t as

$$V\propto\mathcal{D}(\sqrt{\mathcal{D}t})^{h-1-D_B}. \tag{14}$$

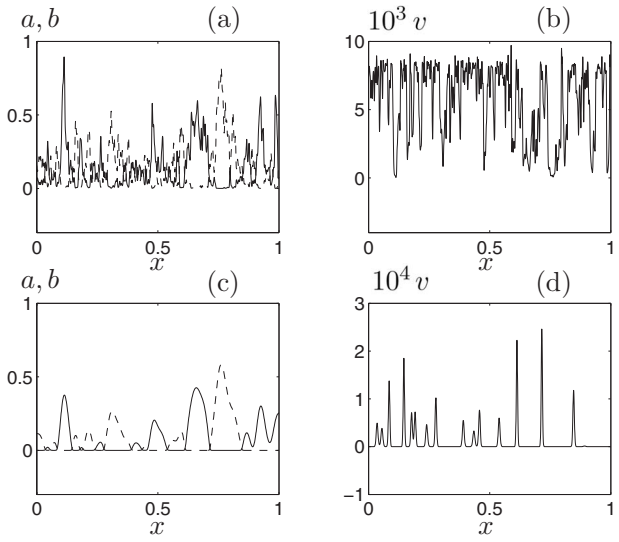

FIG. 2. One-dimensional numerical integration of Eq. (4) with $\mathcal{D}=10^{-7}$ and initial conditions given by Eqs. (15) and (A1) with $\alpha=0.3$. (a) and (c) concentration fields a (—) and b (—) at $t=10$ and 1000, respectively. (b) and (d) local reaction speed $v=ab$ (—) at $t=10$ and 1000, respectively.

The validity of Eqs. (10) and (14) is addressed by comparison with the results of numerical simulations using the numerical scheme presented in Sec. II A. As developed in Appendix A, the self-similar characteristics of the initial concentration fields $a_0(x)$ and $b_0(x)$ are obtained by one-dimensional fractional Brownian motion realizations $f_0(x)$, under the form of Eq. (A1). To retrieve the statistical self-similar properties of fractional Brownian motion, each case is ensemble-averaged over 25 realizations.

The prescription of the initial conditions first allows us to assess the evolution of the system towards the segregation of the reactants. Two cases are considered. On the one hand, the reactants are initially set in contact by prescribing the initial concentrations:

$$a_0(x)=1+2f_0(x)/\max(|f_0(x)|),$$

$$b_0(x)=1-2f_0(x)/\max(|f_0(x)|). \tag{15}$$

Such a case is depicted in Fig. 2 and exhibits the occurrence of the segregation as the reactant initially locally in default is depleted. On the other hand, the reactants are initially segregated by prescribing the initial concentrations:

$$a_0(x)=2\max(f_0(x),0)/\overline{|f_0(x)|},$$

$$b_0(x)=-2\min(f_0(x),0)/\overline{|f_0(x)|}. \tag{16}$$

Such a case is depicted in Fig. 3. The segregation of the reactants and the build up of $\mathcal{B}$ are shown in Figs. 2 and 3 to set in over a similar transient time related to the characteristic reaction time ($t\sim 1$). During this transient, the initially mixed system behaves almost like a perfectly mixed one whereas the initially segregated one does not react. After the transient, Fig. 4 allows one to verify that the reaction almost exclusively occurs on $\mathcal{B}$ and that both $N_{\mathcal{B}}$ and V evolve simi-

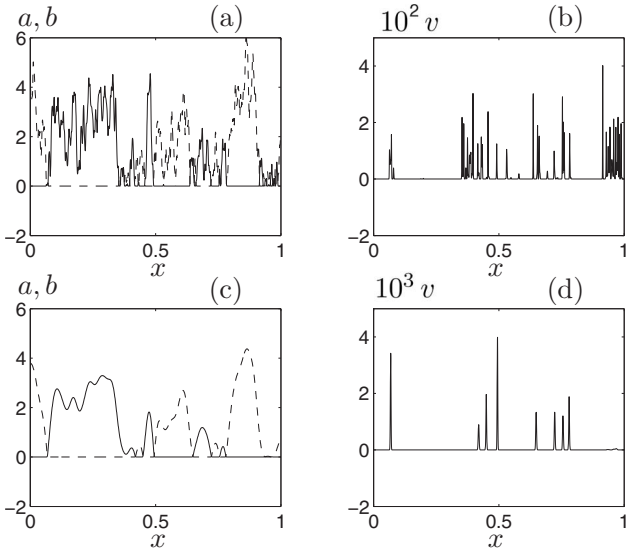

FIG. 3. Same as Fig. 2, but with initial conditions given by Eqs. (16) and (A1).

larly with time, irrespective of the initial conditions. Thus the initial transient is found not to significantly modify the Hölder exponent h of the concentration fields within the patches. Initially segregated concentration fields, Eq. (16), will be used in the forthcoming. We now focus on the algebraic temporal decays of $N_{\mathcal{B}}$ and V observed in Fig. 4 after the transient.

The numerically obtained exponents of the algebraic temporal decays of $N_{\mathcal{B}}$ and V, as functions of α, i.e., the index of the fractional Brownian motion used for the initial conditions, are depicted in Fig. 5. They exhibit a good agreement with the analytical scaling laws Eqs. (10) and (14), reexpressed substituting $D_{\mathcal{B}}=1-\alpha$ and $h=\alpha$. This agreement deteriorates for $\alpha\to 0$, as $\mathcal{B}$ becomes space-filling, and $\alpha\to 1$, as the number of points of $\mathcal{B}$ and the related statistics dwindle.

Beside the temporal behavior, the scaling laws of Eqs. (10) and (14) with respect to diffusivity $\mathcal{D}$ are also of interest. For a given geometry, it allows one to infer the value of V at very small values of $\mathcal{D}$, which is numerically expensive to obtain, from V obtained at, relatively, large values of $\mathcal{D}$. As checked in Fig. 6, the analytical results are again in good

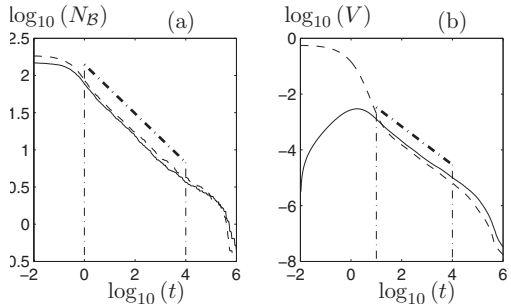

FIG. 4. Comparison between the temporal evolutions of $N_{\mathcal{B}}$ (a) and V (b), ensemble-averaged over 25 realizations, with settings and initial conditions as in Figs. 2 (—) and 3 (—) and corresponding fits of the algebraic decays (–·–).

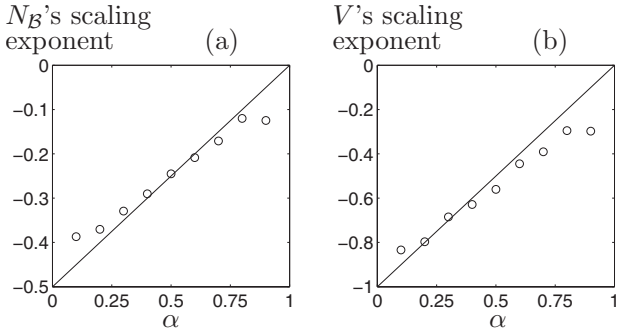

FIG. 5. Exponents of the algebraic temporal decays of $N_{\mathcal{B}}$ (a) and V (b) as functions of α. Comparisons between the analytical scaling laws Eqs. (10) and (14) (—) and the slopes (○) of the numerical fits such as (–·–) in Figs. 4(a) and 4(b).

agreement with the numerical ones. As a matter of fact, no algebraic temporal decay of $N_{\mathcal{B}}$ and V is observed for $\mathcal{D}>10^{-4}$ and, therefore, the assumptions of fast reaction and resulting segregated state are no longer valid.

C. Two-dimensional case

The two-dimensional situation is conceived of as an extension of the one-dimensional case. The boundary $\mathcal{B}$ turns into a set of curves, the "roughness" of which can be quantified by the local curvature radius r_c. A patch of reactant can be seen as a set of inclusions of characteristic sizes r_c. For $r_c \ll \sqrt{\mathcal{D}t}$, the whole corresponding inclusion is under the effect of diffusion, leading to the exponential collapse of the inclusion. At time t the local curvature radius of $\mathcal{B}$ is then assumed to be much larger than $\sqrt{\mathcal{D}t}$. Therefore diffusion is almost one-dimensional and results of Sec. II A still hold. The box-counting dimension $D_{\mathcal{B}}$ and the diffusive cutoff length $\sqrt{\mathcal{D}t}$ govern the length of $\mathcal{B}$. This length is approximated as the number of squares of edge $\sqrt{\mathcal{D}t}$ covering $\mathcal{B}$, multiplied by this resolution, hence

$$L_{\mathcal{B}} \propto (\sqrt{\mathcal{D}t})^{1-D_B}. \tag{17}$$

Moreover, integrating the local diffusive flux Eq. (13) along $\mathcal{B}$ yields the algebraic dependence of V with t and $\mathcal{D}$:

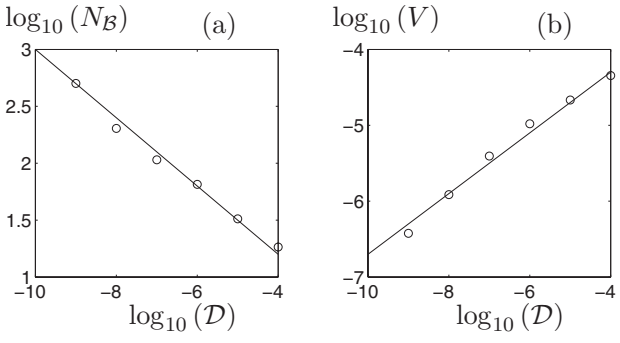

FIG. 6. Algebraic scaling laws of $N_{\mathcal{B}}$ (a) and V (b) with diffusivity $\mathcal{D}$, for $\alpha=0.4$. Comparisons between the analytical scaling laws Eqs. (10) and (14), both up to an arbitrary multiplicative constant (—) and values of $N_{\mathcal{B}}$ and V numerically obtained at $t=1000$ (○).

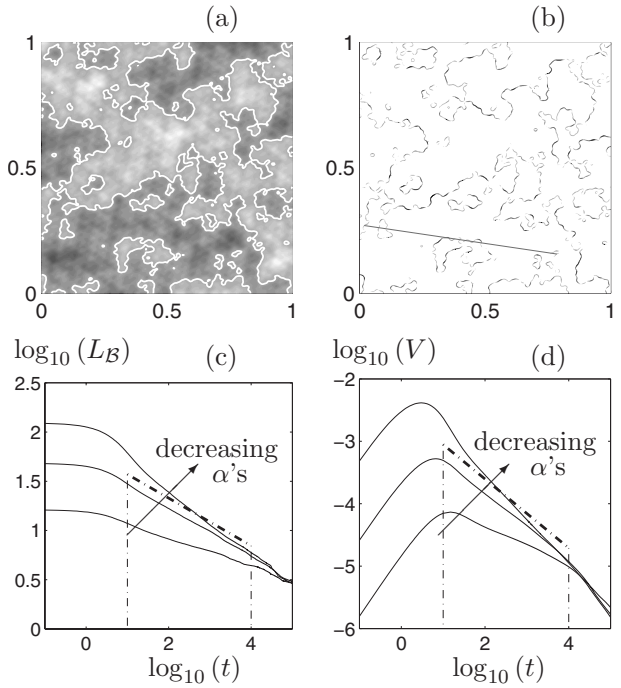

FIG. 7. Two-dimensional numerical integration of Eq. (4) with $\mathcal{D}=10^{-7}$ and initial conditions given by Eqs. (16) and (A1). Snapshots for $\alpha=0.5$ at $t=100$ of (a) $a-b$, with A-rich domain in lighter shades of gray, B-rich domain in darker shades of gray, and $\mathcal{B}$ in white and (b) $v=ab$, with higher values in darker shades of gray. Temporal evolutions of $L_{\mathcal{B}}$ (c) and V (d) for $\alpha=0.75$, 0.5, and 0.25 (decreasing according to the arrow) ensemble-averaged over four realizations and corresponding fits of the algebraic decays (–·–) for $\alpha=0.5$.

$$V \propto \mathcal{D}(\sqrt{\mathcal{D}t})^{h-D_{\mathcal{B}}}. \tag{18}$$

Numerically, the two-dimensional diffusion-reaction system Eq. (4) is solved by a first order forward-time centered-space scheme on a 512×512 grid. Vanishing Neumann boundary conditions are imposed on $x=0,1$ and $y=0,1$. The initial conditions are obtained as the two-dimensional extension of Eq. (16), with $f_0(x,y)$ an index-α fractional Brownian motion obtained by Eq. (A1). The length of $\mathcal{B}$ is numerically evaluated as the number of grid-cells covering the boundary multiplied by the grid precision $\Delta x=1/512$. This length is not precision-dependent as long as the boundary is resolved and regular at the grid precision, i.e., as long as $\Delta x \ll \sqrt{\mathcal{D}t}$. The length of $\mathcal{B}$ in the two-dimensional cases alleviates the necessity of large statistics of the one-dimensional case, the ensemble average is therefore reduced to four realizations. Such a numerical simulation and the observed algebraic temporal decays of $L_{\mathcal{B}}$ and V are depicted in Fig. 7.

The numerically obtained exponents of these algebraic temporal decays of $L_{\mathcal{B}}$ and V, as functions of α, are depicted in Fig. 8. They are again in good agreement with the analytical scaling laws Eqs. (17) and (18), reexpressed substituting $D_{\mathcal{B}}=2-\alpha$ and $h=\alpha$.

It should be noted that Eq. (14) is similar, for $\alpha \leqslant 1/2$, to expressions obtained in discrete reaction-subdiffusion systems, with a subdiffusive process then described by a mean square displacement $\langle r^2(t)\rangle \propto t^{2\alpha}$ and notwithstanding the peculiar treatment of the reaction term in the discrete framework required by the subdiffusion operator used in Monte Carlo numerical simulations [14]. Nevertheless, as said in Sec. I, the relation between discrete and mean-field approaches is left beyond the scope of this paper.

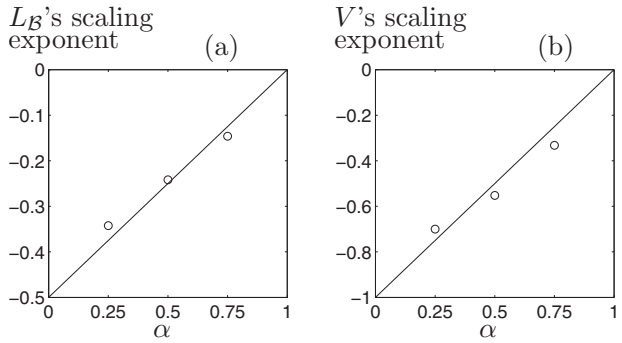

FIG. 8. Exponents of the algebraic temporal decays of $L_{\mathcal{B}}$ (a) and V (b) as functions of α. Comparisons between the analytical scaling laws Eqs. (17) and (18) (—) and the slopes (○) of the numerical fits such as (–·–) in Fig. 7(c) and 7(d).

III. ADVECTION-DIFFUSION-REACTION IN A SINGULAR VORTEX

Advection-diffusion-reaction is now considered. The singularity originates from the advection of the reactants by a two-dimensional steady vortex. Such a vortex presents an orthoradial flow in the form

$$u_\theta(r) = \frac{1}{\mathrm{Da}} r^{-\beta}, \tag{19}$$

where $1/\mathrm{Da}$ scales the velocity at $r=1$. Flows given by Eq. (19) are easily checked to be shear flows. Without elaborating much further on the vortex dynamics itself, vortices with $\beta \neq 1$ are an interesting generalization of the isolated point vortex $\beta=1$ as the exponent β can take into account modifications of the strong vortical velocity field due to an embedding weak vorticity in two-dimensional turbulence, as presented in [17]. Moreover, flows satisfying Eq. (19) with $\beta \neq 1$ are also observed between two porous rotating cylinders [43] or in trailing vortices behind airfoils [44].

A. Advection and diffusion of a patch advected by a vortex

The effect of a vortex on a patch of scalar is due to the combined action of differential orthoradial shear and radial accumulation of the plies of the spiral generated. Considering, as sketched in Fig. 9, the advection of a material patch of initially radial length dl_0 and initially orthoradial width ds_0, located at distance r from the center of the vortex, the differential velocity leads to the stretching of the patch. The direction of the stretched length of the patch is denoted by l and the direction of its contracting width by s. The evolution of the length of the patch is given by

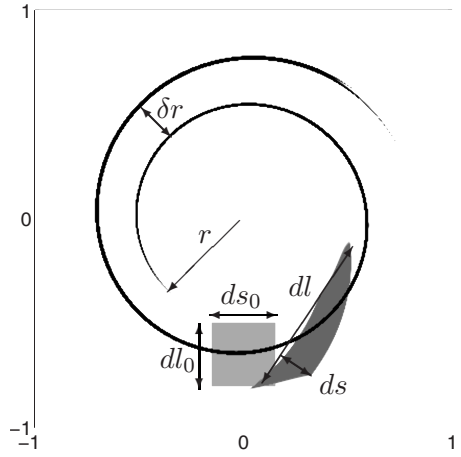

FIG. 9. Sketched evolution of a patch advected by a singular vortex, with increasing times in darker shades of gray.

$$dl = \sqrt{1 + \left(r\frac{d\theta}{dr}\right)^2}\, dl_0 = \sqrt{1 + \left((\beta+1)\frac{t}{\mathrm{Da}} r^{-\beta-1}\right)^2}\, dl_0 = \sqrt{1+\mathcal{S}^2}\, dl_0, \tag{20}$$

with strain $\mathcal{S}=rd\theta/dr=(\beta+1)r^{-\beta-1}t/\mathrm{Da}$ introduced and used hereinafter for the sake of clarity. The divergence-free velocity field implies the conservation of the area of the patch while it is advected. Consequently, its width evolves as

$$ds = (\sqrt{1+\mathcal{S}^2})^{-1} ds_0. \tag{21}$$

Also on a kinematic point of view, at fixed radius r and time t, the advection of an initially radial material line by the vortex generates two plies at a distance

$$\delta r = \frac{2\pi}{d\theta/dr} = \frac{2\pi}{\beta+1}\frac{\mathrm{Da}}{t} r^{\beta+2}. \tag{22}$$

Considering now that the patch is filled with a passive scalar, taking diffusion into account can be done using the analysis introduced by Ranz [45] and used, for instance, by Meunier and Villermaux [22] in the case $\beta=1$. Diffusion along the l-direction is neglected and the change of variables $(s,t)\to(\sigma,\tau)$ such as

$$\tau = t + \mathcal{S}^2\frac{t}{3},$$

$$\sigma = (1+\mathcal{S}^2)^{1/2} s \tag{23}$$

is introduced. This turns the advection-diffusion equation satisfied by $f=a-b$, $\partial_t f+\boldsymbol{u}\cdot\boldsymbol{\nabla} f=\mathcal{D}\Delta f$ into a one-dimensional diffusion equation $\partial_\tau f=\mathcal{D}\partial_\sigma^2 f$.

As V is expected to increase with L_B, it is sound to focus on the part of the region where material lines are noticeably stretched by the vortex and almost aligned with the shear direction. The patch presents there a spiraled structure. At fixed radius r, this is obtained after the characteristic time $t=\mathrm{Da}r^{\beta+1}/(\beta+1)$. Equivalently, at time t, the spiral is observed within the outer circle $\mathcal{C}_{\mathrm{out}}$ of radius

$$r_{\mathrm{out}} = \left((\beta+1)\frac{t}{\mathrm{Da}}\right)^{1/(\beta+1)} \propto \left(\frac{t}{\mathrm{Da}}\right)^{1/(\beta+1)}. \tag{24}$$

In the spiraled region, $\mathcal{S}>1$ and Eqs. (20), (21), and (23) simplify into

$$dl = \mathcal{S} dl_0, \tag{25}$$

$$ds = \mathcal{S}^{-1} ds_0 \tag{26}$$

and

$$\tau = \mathcal{S}^2\frac{t}{3},$$

$$\sigma = \mathcal{S}s. \tag{27}$$

Diffusion smooths out the plies of the generated spiral close to the center of the vortex where they tend to accumulate. Perpendicular to the shear, therefore to $\mathcal{B}$ in the spiraled region, the characteristic diffusive length scale $\sqrt{\mathcal{D}t}$, obtained in absence of advection, is retrieved. This smoothed-out region is observed where the distance between two plies, δr given by Eq. (22), decreases below $\sqrt{\mathcal{D}t}$. This occurs within the inner circle $\mathcal{C}_{\mathrm{in}}$ of radius

$$r_{\mathrm{in}} = \left(\frac{\beta+1}{\pi}\frac{t}{\mathrm{Da}}\sqrt{\mathcal{D}t}\right)^{1/(\beta+2)} \propto \left(\frac{t}{\mathrm{Da}}\sqrt{\mathcal{D}t}\right)^{1/(\beta+2)}. \tag{28}$$

For all positive value of β, r_{out} in Eq. (24) grows faster than r_{in} in Eq. (28). It must, however, be kept in mind that the extension of the spiral and its smoothing-out occur simultaneously and not sequentially as assumed in [19].

B. Orders of magnitude for quantities associated with $\mathcal{B}$

Using the change of variables Eq. (27), the scaling laws Eqs. (7) and (8), obtained in absence of advection for, respectively, $s_{\mathcal{B}}$ the characteristic width of the reactive band centered on $\mathcal{B}$ and $c_{\mathcal{B}}$ the characteristic concentration within this band, can be extended to this case of advection-diffusion-reaction along a boundary advected by a vortex. Dropping from now on the coefficients of order unity and focusing on the dependence with time and the physical parameters, it yields, at fixed location $r<r_{\mathrm{out}}$:

$$s_{\mathcal{B}} \sim \mathcal{S}^{-2/3}\left(\frac{\mathcal{D}\sqrt{\mathcal{D}t}}{C}\right)^{1/3} \tag{29}$$

and

$$c_{\mathcal{B}} \sim \mathcal{S}^{-2/3}\left(\frac{\mathcal{D}C^2}{\sqrt{\mathcal{D}t}}\right)^{2/3}, \tag{30}$$

with C the characteristic concentration in a patch. Owing to the $\mathcal{S}^{-2/3}$ factor in Eqs. (29) and (30), at fixed r and for long times, the assumptions that the reactive band reduces to $\mathcal{B}$ and that the concentrations of the reactants vanish on $\mathcal{B}$ remain justified. The displacement of the boundary is now assumed to be due exclusively to the advection by the vortex, as it would be for a material line.

C. Patches of initial constant concentrations

The situation where the two reactants A and B are initially separated in two half-spaces, with, respectively, $a_0=1, b_0=0$ and $a_0=0, b_0=1$ (i.e., presenting a Hölder exponent $h=0$) is considered. The boundary $\mathcal{B}$, which initially coincides with the line between the two half-spaces is advected by the velocity field Eq. (19). The generated two-arm spiral within $\mathcal{C}_{\text{out}}$ presents a specific box-counting dimension related to β. According to [46], the box-counting dimension of a one-dimensional cut through the spiral is $D_{\mathcal{B}\text{cut}}=(\beta+1)/(\beta+2)$. Owing to the accumulation of its plies around the center of the vortex, the whole spiral exhibits a box-counting dimension

$$D_{\mathcal{B}} = \frac{2\beta+2}{\beta+2}, \tag{31}$$

double of $D_{\mathcal{B}\text{cut}}$, as it is retrieved in Appendix B. This result holds irrespective of the initial position of the material line. Given the integral scale r_{out} given by Eq. (24) and the self-similar structure of the expanding spiral, the number of squares of edge ε required to cover the spiral reads

$$N(\varepsilon) = \left(\frac{\varepsilon}{r_{\text{out}}}\right)^{-D_B}. \tag{32}$$

Under the effect of radial diffusion, the length of $\mathcal{B}$ is thus approximated by

$$L_{\mathcal{B}} \propto \sqrt{\mathcal{D}t}\left(\frac{\sqrt{\mathcal{D}t}}{r_{\text{out}}}\right)^{-(2\beta+2)/(\beta+2)} \propto (\sqrt{\mathcal{D}t})^{-\beta/(\beta+2)}\left(\frac{t}{\text{Da}}\right)^{2/(\beta+2)}. \tag{33}$$

Multiplying this length by the diffusive flux $\mathcal{D}/\sqrt{\mathcal{D}t}$ across $\mathcal{B}$, obtained for initial on/off concentration fields, leads to the algebraic temporal evolution of V in the spiraled region:

$$V \propto \mathcal{D}\left(\frac{\sqrt{\mathcal{D}t}}{r_{\text{out}}}\right)^{-(2\beta+2)/(\beta+2)} \propto \mathcal{D}(\sqrt{\mathcal{D}t})^{-(2\beta+2)/(\beta+2)}\left(\frac{t}{\text{Da}}\right)^{2/(\beta+2)}. \tag{34}$$

The validity of Eqs. (33) and (34) is evaluated by comparison with the results of the numerical integration of Eq. (3) by a fourth order Runge-Kutta compact scheme associated with periodic boundary conditions. The vortex imposed in the simulation presents a "solid rotation" core to prevent diverging velocities. Furthermore, in the numerical simulations the vortex and the associated spiral live in the finite-size domain $[-1,1]\times[-1,1]$. Equations (33) and (34) can be compared with the numerical results as long as the spiral does not reach the limit of the domain, i.e., as long as $t<\text{Da}$. In simulations, $\mathcal{B}$ intersects the center of the vortex. Such a numerical simulation and the observed algebraic temporal evolutions of $L_{\mathcal{B}}$ and V are depicted in Fig. 10. As seen in Fig. 11, the results obtained numerically for the exponents of the temporal scaling laws as functions of β compare very favorably with the analytical scaling laws Eqs. (33) and (34), notwithstanding a noticeable deterioration for small β's. Equation (33) implies that the length of the spiraled $\mathcal{B}$ generated by a vortex with $\beta>4$ asymptotically tends to decrease as more length is removed along the inner plies by diffusion than generated by the outer extension of the spiraled region. Even though numerical simulations have not been attempted for $\beta>3$ due to numerical costs, this result is compatible with Fig. 10(c).

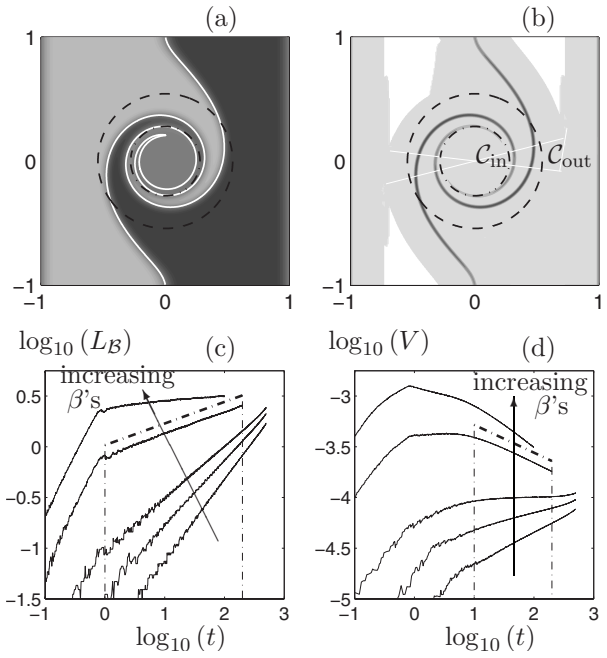

FIG. 10. Numerical integration of Eq. (3) with velocity field Eq. (19), $\mathcal{D}=10^{-5}$ and $\text{Da}=10^3$. Snapshot for $\beta=2$ at $t=160$ of (a) $a-b$, with A-rich domain in lighter shades of gray, B-rich domain in darker shades of gray, and $\mathcal{B}$ in white and (b) $v=ab$, with higher values in darker shades of gray, $\mathcal{C}_{\text{in}}$ (–·–) and $\mathcal{C}_{\text{out}}$ (– –) superimposed. Temporal evolutions of $L_{\mathcal{B}}$ (c) and V (d) for $\beta=0.5$, 0.75, 1,2, and 3 (increasing according to the arrow) integrated within $\mathcal{C}_{\text{out}}$ and corresponding fits of the algebraic growths (–·–) for $\beta=2$.

IV. INITIALLY SELF-SIMILAR CONCENTRATION FIELDSADVECTED BY A SINGULAR VORTEX

Self-similarity of the concentration fields and singularity of the vortex are now combined. Initial concentration fields

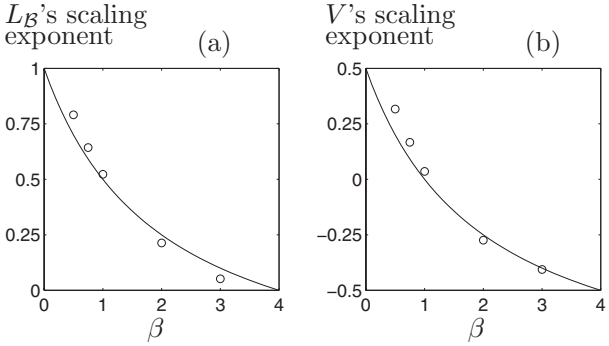

FIG. 11. Exponents of the algebraic temporal evolutions of $L_{\mathcal{B}}$ (a) and V (b) as functions of β. Comparisons between the analytical scaling laws Eqs. (33) and (34) (—) and the slopes (○) of the numerical fits such as (–·–) in Figs. 10(c) and 10(d).

characterized by a Hölder exponent h_0 and a box-counting dimension of $\mathcal{B}$, $D_{\mathcal{B}_0}$ are advected by the velocity field Eq. (19). Considering an inclusion of reactant, located on $\mathcal{C}_r$ the circle of radius r, its initial length dl_0 and width ds_0 (see Fig. 9) evolve according to Eqs. (25) and (26). Owing to the radial diffusion of reactants, this inclusion disappears when its width ds is reduced below $\sqrt{\mathcal{D}t}$. From Eq. (26), this involves inclusions of initial width $ds_{0,\text{smoothed-out}} \propto \mathcal{S}\sqrt{\mathcal{D}t}$. At fixed r and t, the number of times the boundary $\mathcal{B}$ intersects $\mathcal{C}_r$ is equal to the number of times $\mathcal{B}$, with a cutoff length $ds_{0,\text{smoothed-out}}$, initially intersects $\mathcal{C}_r$. This number is expressed as a function of $D'_{\mathcal{B}_0}=D_{\mathcal{B}_0}-1$, the box counting dimension of the intersection $\mathcal{B}\cap\mathcal{C}_r$ at $t=0$:

$$N_{\mathcal{B}\cap\mathcal{C}_r} \propto r(ds_{0,\text{smoothed-out}})^{-D'_{\mathcal{B}_0}} \propto r(\mathcal{S}\sqrt{\mathcal{D}t})^{1-D_{\mathcal{B}_0}}. \quad (35)$$

Diffusion smooths out the reactants, leaving a single—nonreactive—inclusion, for $r<r_{\text{in}}$ with r_{in} given by Eq. (28). Using Eq. (25), between $\mathcal{C}_r$ and $\mathcal{C}_{r+dr}$ each of these inclusions and corresponding boundaries contributes to the length of $\mathcal{B}$ by $dl=\mathcal{S}dr$. Hence the length of $\mathcal{B}$ evolves as

$$L_{\mathcal{B}} \propto \int_{r_{\text{in}}}^{r_{\text{out}}} \left(r^{-\beta-1}\frac{t}{\text{Da}}\sqrt{\mathcal{D}t}\right)^{1-D_{\mathcal{B}_0}} \times r^{-\beta}\frac{t}{\text{Da}}dr. \quad (36)$$

Two situations are to be considered. For $D_{\mathcal{B}_0}>2\beta/(\beta+1)$, the temporal evolution of $L_{\mathcal{B}}$ is governed by the increase of the number of boundary points given by Eq. (35), larger as $\mathcal{C}_r\to\mathcal{C}_{\text{out}}$:

$$L_{\mathcal{B}} \propto (\sqrt{\mathcal{D}t})^{1-D_{\mathcal{B}_0}}\left(\frac{t}{\text{Da}}\right)^{2/(\beta+1)}. \quad (37)$$

For $D_{\mathcal{B}_0}<2\beta/(\beta+1)$, the temporal evolution of $L_{\mathcal{B}}$ is governed by the accumulation of the plies of $\mathcal{B}$ as $\mathcal{C}_r\to\mathcal{C}_{\text{in}}$:

$$L_{\mathcal{B}} \propto (\sqrt{\mathcal{D}t})^{(2-\beta-D_{\mathcal{B}_0})/(\beta+2)}\left(\frac{t}{\text{Da}}\right)^{(4-D_{\mathcal{B}_0})/(\beta+2)}. \quad (38)$$

The marginal case $D_{\mathcal{B}_0}=2\beta/(\beta+1)$ leads to

$$L_{\mathcal{B}} \propto (\sqrt{\mathcal{D}t})^{1-D_{\mathcal{B}_0}}\left(\frac{t}{\text{Da}}\right)^{2-D_{\mathcal{B}_0}} \times\left[\ln\left(\frac{t}{\text{Da}}\right)^{1/(\beta+1)} - \ln\left(\sqrt{\mathcal{D}t}\frac{t}{\text{Da}}\right)^{1/(\beta+2)}\right]. \quad (39)$$

The global reaction speed is evaluated in a similar fashion by integrating the diffusive flux along $\mathcal{B}$. Equation (13), obtained for pure diffusion, is reexpressed using the change of variable Eq. (27) to take the shear into account, leading to $\mathcal{D}|\partial_x f(0,t)| \propto \mathcal{D}\mathcal{S}^{h_0}(\sqrt{\mathcal{D}t})^{h_0-1}$. For $h_0\neq 0$, the shear modifies the diffusive flux. Moreover, in the case of the vortex the shear varies with r. Hence the global reaction speed can no longer be straightforwardly obtained by multiplying the length of $\mathcal{B}$ by the average value of the flux, but must be obtained by integrating this total flux. The global reaction speed, integrated over the spiraled region, then follows:

$$V \propto \int_{r_{\text{in}}}^{r_{\text{out}}} \left(r^{-\beta-1}\frac{t}{\text{Da}}\right)^{1+h_0-D_{\mathcal{B}_0}} (\sqrt{\mathcal{D}t})^{1-D_{\mathcal{B}_0}} \times r^{-\beta}\frac{t}{\text{Da}}dr. \quad (40)$$

Hence for $D_{\mathcal{B}_0}-h_0>2\beta/(\beta+1)$, V is governed by $\mathcal{C}_{\text{out}}$, where $\mathcal{S}=1$:

$$V \propto \mathcal{D}(\sqrt{\mathcal{D}t})^{h_0-D_{\mathcal{B}_0}}\left(\frac{t}{\text{Da}}\right)^{2/(\beta+1)} \quad (41)$$

and for $D_{\mathcal{B}_0}-h_0<2\beta/(\beta+1)$, V is governed by $\mathcal{C}_{\text{in}}$:

$$V \propto \mathcal{D}(\sqrt{\mathcal{D}t})^{(4+h_0-D_{\mathcal{B}_0})/(\beta+2)-2}\left(\frac{t}{\text{Da}}\right)^{(4+h_0-D_{\mathcal{B}_0})/(\beta+2)}. \quad (42)$$

The marginal case $D_{\mathcal{B}_0}-h_0=2\beta/(\beta+1)$ leads to

$$V \propto (\sqrt{\mathcal{D}t})^{h_0-D_{\mathcal{B}_0}}\left(\frac{t}{\text{Da}}\right)^{2+h_0-D_{\mathcal{B}_0}} \times\left[\ln\left(\frac{t}{\text{Da}}\right)^{1/(\beta+1)} - \ln\left(\sqrt{\mathcal{D}t}\frac{t}{\text{Da}}\right)^{1/(\beta+2)}\right]. \quad (43)$$

The analytical scaling laws Eqs. (37), (38), (41), and (42) are compared with the results of numerical simulations using the numerical scheme of Sec. III C, with initial concentration fields prescribed using fractional Brownian motion as in Sec. II C. The vortex being a strongly localized structure, retrieving the statistical features of the fractional Brownian motion requires large statistics, hampered by high computational costs. The present results were obtained by averaging over eight realizations for each case. An example of the evolutions of the concentrations and local reaction term is depicted in Fig. 12 together with the temporal evolutions of $L_{\mathcal{B}}$ and V. The validity of the analytical scaling laws Eqs. (37) and (38) for $L_{\mathcal{B}}$ and Eqs. (41) and (42) for V, reexpressed substituting $D_{\mathcal{B}_0}=2-\alpha$, and $h_0=\alpha$ is checked in Fig. 13. Despite the obvious need for larger statistics they exhibit a good agreement between numerical simulations and analytical scaling laws.

V. DISCUSSION

Two points tackled in the previous sections are now discussed in more detail. First, the results obtained in Secs. II–IV are compared in the light of the temporal evolution of the global reaction speed V for the different situations. Then, we will focus on peculiar characteristics inferred from Sec. IV of initially self-similar concentration fields advected by a vortex.

A. Global reaction speeds

The comparison is done for a globally stoichiometric system. Comparing the different global reaction speeds does not assess the total yields of the reaction—i.e., the average concentrations of products—in the system, as they strongly depend on the transient state. Results on the exponents of the algebraic temporal evolution of V, obtained for the various situations addressed in this paper, are summarized in Table I and are now discussed further.

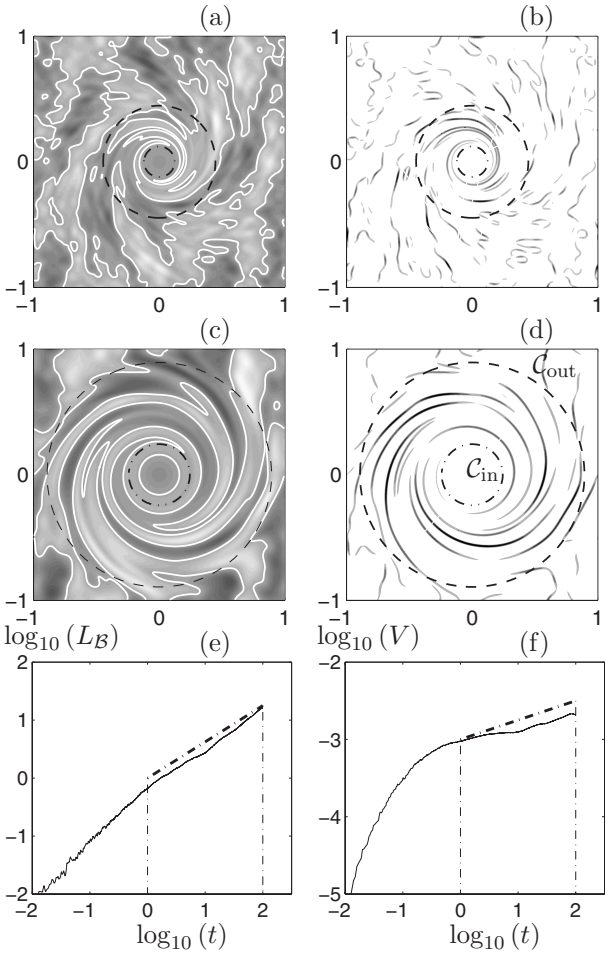

FIG. 12. Numerical integration of Eq. (3) for velocity field Eq. (19) with $\beta=1$, $\mathcal{D}=10^{-5}$, $\mathrm{Da}=10^{2}$ and initial conditions given by Eqs. (16) and (A1) with $\alpha=0.25$. Snapshot at $t=20$ of (a) $a-b$, with A-rich domain in lighter shades of gray, B-rich domain in darker shades of gray, and $\mathcal{B}$ in white and (b) $v=ab$, with higher values in darker shades of gray, $\mathcal{C}_{\text{out}}$ and $\mathcal{C}_{\text{in}}$ superimposed. (c) Same as (a) at $t=80$. (d) Same as (b) at $t=80$. Temporal evolutions of $L_{\mathcal{B}}$ (e) and V (f) ensemble-averaged over eight realizations (—) and corresponding fits of the algebraic evolutions (–·–).

With perfectly premixed reactants (case ① in Table I), V asymptotically exhibits the algebraic decay t^{-2} due to the second order reaction. The fluctuations of the concentrations of the reactants and their advection by an imposed velocity field tend to deeply modify this temporal evolution for fast reaction, as the reaction is now diffusion-limited. As a first consequence of the diffusive nature, due to the finite size of the domain, an algebraic behavior can only be observed for $t \ll \mathcal{D}^{-1}$, where $\mathcal{D}$ is the diffusivity, nondimensionalized as stated in Eq. (3), i.e., as long as diffusivity does not influence the whole physical domain.

Without advection, the crudest model of segregation consists of two A-rich and B-rich subdomains of initially constant concentrations, separated by a $\mathcal{B}$ keeping a fixed length (case ② in Table I). The global reaction speed, namely the diffusive flux integrated along $\mathcal{B}$, asymptotically scales as $(\mathcal{D}t)^{-1/2}$.

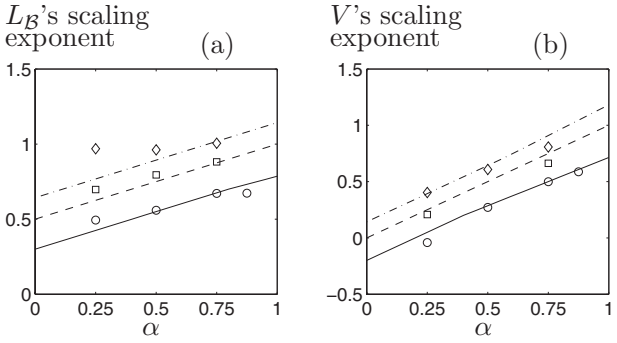

FIG. 13. Exponents of the algebraic temporal evolutions of $L_{\mathcal{B}}$ (a) and V (b) as functions of α and β. Comparisons between the analytical scaling laws Eqs. (37) and (38) and Eqs. (41) and (42), respectively, for $\beta=0.75$ (–·–), 1 (– –), and 1.5 (—) and the slopes of the numerical fits such as (–·–) in Fig. 12(e) and 12(f), respectively, also for $\beta=0.75$ (◇), 1 (□), and 1.5 (○).

Still without advection, singular fluctuations of the reactants are handled using this segregated state, in the form of $\mathcal{B}$ presenting a box-counting dimension $2>D_{\mathcal{B}}>1$ and the concentrations of a Hölder exponent $1>h>0$ (case ③ in Table I). The algebraic temporal evolution of V Eq. (18) is then always found to decay more slowly than t^{-1}. The fastest decay is obtained for $D_{\mathcal{B}}=2$ and $h=0$. For large values of h, V may exhibit a temporal growth. Nevertheless this regime is only inferred and could not be obtained numerically as the fractional Brownian motion used for the initial conditions introduces a link between h and $D_{\mathcal{B}}$.

The validity of the segregated state is then extended to advection-diffusion-reaction in the case of steady vortices, with the orthoradial velocity scaling as $r^{-\beta}$, advecting a single boundary between two A-rich and B-rich subdomains of initially constant concentrations (case ④ in Table I). For such a vortex living in a fixed domain, the asymptotic behavior holds as long as $t \ll \mathrm{Da}$, where Da is the Damköhler number nondimensionalized as stated in Eq. (3), i.e., as long as $\mathcal{C}_{\text{out}}$ remains in the finite-size domain. Depending on the value of β, V in Eq. (34) asymptotically exhibits an algebraic decrease ($\beta<1$) or increase ($\beta>1$). The decay of V is always found slower than t^{-1}. For the isolated point vortex case $\beta=1$, the growth of the length $L_{\mathcal{B}}$ balances the decline of the diffusive flux and V saturates at a constant value. The results obtained and depicted in Fig. 10 for $\mathcal{B}$ intersecting the

TABLE I. Comparison between the exponents of the algebraic temporal evolution of V for different cases tackled analytically and numerically and validity domains of the algebraic scaling laws.

Case	V's scaling exponent	Validity
①: Perfectly premixed	-2	$1 \ll t$
②: Fixed subdomains	$-1/2$	$1 \ll t \ll \mathcal{D}^{-1}$
③: Fractional Brownian motion	$-1<\cdots<0$	$1 \ll t \ll \mathcal{D}^{-1}$
④; Vortex	$-1<\cdots<1/2$	$1 \ll t \ll \mathrm{Da}$
⑤: Vortex and fractional Brownian motion	$-1<\cdots<2$	$1 \ll t \ll \mathrm{Da}$

center of the vortex still hold for $\mathcal{B}$ initially at distance d from the center. The system then presents a nonreactive core region of radius d and the algebraic regime will be observed for $t \gg (d^{\beta+2}\mathrm{Da}/\sqrt{\mathcal{D}})^{2/3}$. Finally, it is reminded that Eq. (34) describes the behavior of V, integrated over the spiraled domain, within $\mathcal{C}_{\mathrm{out}}$, and not in the whole domain. Nevertheless, this spiraled domain being the main contribution to the total length of $\mathcal{B}$, Eq. (34) can be considered as the global reaction speed in the whole domain.

Self-similar initial conditions and singularity stemming from an imposed vortex are now combined (case ⑤ in Table I). Considering initial concentration fields characterized by an initial Hölder exponent $h_0 > 0$ and $\mathcal{B}$ by an initial box-counting dimension $2 > D_{\mathcal{B}_0} > 1$, the algebraic scaling laws for V Eqs. (41) and (42) are deduced. As for the previous case, the algebraic scaling law is observed for $t \ll \mathrm{Da}$. The global reaction speed is found to follow two possible behaviors. For $D_{\mathcal{B}_0} - h_0 < 2\beta/(\beta+1)$ Eq. (42) holds and the evolution of V is governed by the inner part of the spiral, where the folding effect of the vortex is balanced by diffusion. For $D_{\mathcal{B}_0} - h_0 > 2\beta/(\beta+1)$, Eq. (41) holds and the evolution of V is governed by the extension of the fringe of the spiral over the initially still domain. Once again, the asymptotic regime of V is always found to decay more slowly than t^{-1}. Equations (41) and (42) describe the behavior of V integrated over the spiraled region and, unlike the previous case, a noticeable contribution to V integrated over the whole domain is provided by the outer, unspiraled, region. For this contribution pertaining to diffusion-reaction systems, no algebraic scaling law for V integrated over the whole domain should be recovered. Nevertheless, cases with $D_{\mathcal{B}_0} - h_0 > 2\beta/(\beta+1)$ exhibit a surprising behavior. Indeed, the length of $\mathcal{B}$, Eq. (37), can be recast in the form $L_{\mathcal{B}} \propto (\sqrt{\mathcal{D}t})^{1-D_{\mathcal{B}_0}} r_{\mathrm{out}}^2$, highlighting the fact that the evolution of this length is governed by the length of the initial $\mathcal{B}$ engulfed in the expanding spiraled region. On $\mathcal{C}_{\mathrm{out}}$, $\mathcal{B}$ is advected without being noticeably stretched and the growth of $L_{\mathcal{B}}$ is accounted for by the growth of the spiraled region. The corresponding V, given by Eq. (41), leads to the average reaction speed in the spiraled region $\bar{v} \propto \mathcal{D}(\sqrt{\mathcal{D}t})^{h_0 - D_{\mathcal{B}_0}}$, namely the average reaction rate deduced from Eq. (18) for diffusion-reaction systems and, therefore, valid in the outer, unspiraled, region. The vortex is then found to have no effect on the temporal evolution of the reaction speed integrated over the whole domain. This latter is solely governed by the initial fluctuations of the concentration fields. This result is obtained in the situation of a steady, isolated vortex living in a domain of fixed size and advecting homogeneously self-similar concentration fields.

Compared with the perfectly premixed situation, the multiscale properties of the fluctuations of concentration slow down the temporal decay of V by preventing the reactants to be set in contact. After some critical time, V could hence be higher for stirred nonpremixed situations than for perfectly premixed ones.

As a point of comparison, it should be noted that Eq. (18) with $h=0$ and Eq. (34) are in agreement with previous results by Wonhas and Vassilicos [47,48], establishing in the case of on/off concentration fields that $V \propto -\partial_t f^2 \propto t^{-1}(t\sqrt{\mathcal{D}t}/\Lambda)^{2-D_{\mathcal{B}}}$, with $f = a - b$.

B. More discussion and outlook

The combination of the two sources of singularity in Sec. IV leads to interesting results concerning the reactive and the underlying mixing properties of the situation. First, no interpretation involving a box-counting dimension, as obtained in Secs. II and III, could be found to account for the evolution of $L_{\mathcal{B}}$. This should be related to the different natures of the singularities: global for the self-similar initial conditions and localized for the vortical flow.

Then, for the intermediate regime $2\beta/(\beta+1) + h_0 > D_{\mathcal{B}_0} > 2\beta/(\beta+1)$, the evolutions of $L_{\mathcal{B}}$ and V follow, respectively, Eqs. (37) and (42). The area of generation of $\mathcal{B}$, close to $\mathcal{C}_{\mathrm{out}}$, is found to differ from the area of chemical activity, close to $\mathcal{C}_{\mathrm{in}}$. This fact calls into question the idea that the global reaction speed can be evaluated in a practical situation by first tracking $\mathcal{B}$ and then integrating an averaged diffusive flux along the boundary. This assumption lies behind the crudest "lamellar models" of reactive patches, where the effect of the flow on $\mathcal{B}$ is introduced by the means of an average stretching rate (see, for instance, the discussion in [36] and references therein). It should be also noted that for a point-vortex with $\beta=1$, using Brownian motion ($\alpha=0.5$) for the initial conditions leads to the marginal—nonalgebraic—expression Eq. (43) for V, explaining the absence of the corresponding point in Fig. 13.

Finally, the idea that the proposed approach could mimic a large scale vortex acting on underlying turbulently advected concentration fields must be modified. Indeed, it assumes that the transport properties of the reactants are not dramatically modified by the underlying turbulent flow and are fairly well captured by an eddy-diffusivity coefficient $\mathcal{D}$. Furthermore, the concentration fields can hardly be described by single-valued, stationary $D_{\mathcal{B}}$ and h. The extension of such an approach to spectra of exponents $D_{\mathcal{B}}$, h, and β, in a multifractal fashion [49], constitutes an open and interesting question. Nevertheless, the validation of the analytical results by comparison with numerical simulations would require a tremendous amount of computation.

ACKNOWLEDGMENTS

We would like to acknowledge very helpful discussions with and comments from Pierre Borgnat, Philippe Carrière, Stéphane G. Roux, and Florence Raynal. This work has been supported by the EU Research Training Network "Fluid Mechanical Stirring and Mixing: the Lagrangian Approach" HPRN-CT-2002-00300.

APPENDIX A: PRESCRIPTION OF SELF-SIMILAR INITIAL CONDITIONS IN THE NUMERICAL SIMULATIONS

Self-similarity is introduced in numerical simulations of Secs. II and IV by implementing fractional Brownian motion [50] to prescribe the initial concentration fields. This Gaussian process is such that for every $\boldsymbol{x}$ and $\boldsymbol{\varepsilon}$, the increment $f(\boldsymbol{x}+\boldsymbol{\varepsilon}) - f(\boldsymbol{x})$ has a normal distribution with zero mean and variance $|\boldsymbol{\varepsilon}|^{2\alpha}$. $0 < \alpha < 1$ is an arbitrary index. This process presents a strong self-similarity. First the moments of the

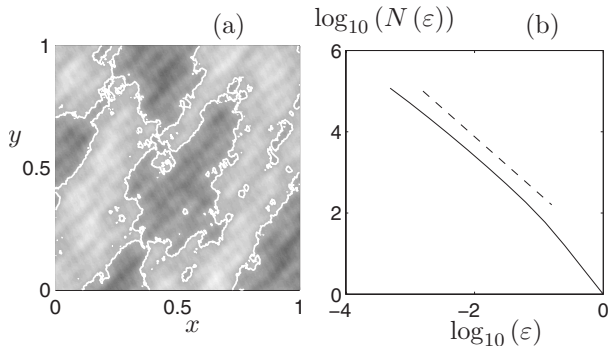

FIG. 14. (a): Realization of two-dimensional fractional Brownian motion by Eq. (A1), with $\alpha=0.6$, $\lambda=1.08$ and $N=150$. The white curve is the zero-crossing set. (b): Evolution of $N(\varepsilon)$ the number of squares required to cover this zero-crossing set, as a function of the length of their edge ε (—), ensemble-averaged over 16 realizations of (a) and compared with the analytical scaling law $\varepsilon^{\alpha-1}$ (– –).

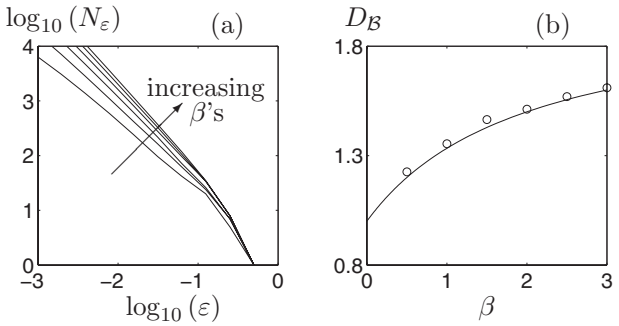

FIG. 15. (a) Number $N(\varepsilon)$ of squares of size ε required to cover the spiral generated by a material line advected by a vortex, as a function of ε, for β ranging from 0.5 to 3 by 0.5 steps (increasing according to the arrow). (b) Comparison between analytical expression Eq. (31) (—) and numerical results (○) for the box-counting dimension $D_{\mathcal{B}}$, the numerical exponents are obtained from (a).

increments of such sample functions exhibiting the scaling law $\overline{|f(\boldsymbol{x}+\boldsymbol{\varepsilon})-f(\boldsymbol{x})|^q} \propto |\boldsymbol{\varepsilon}|^{\alpha q}$, the process presents a Hölder exponent $h=\alpha$. Second, the box-counting dimension of the level-sets $f(\boldsymbol{x})=$const is directly related to α by $D_B=d-\alpha$, where d is the Euclidean dimension of $\boldsymbol{x}$.

On a practical point of view, fractional Brownian motion is approximated by randomized Weierstrass functions in the form

$$f(\boldsymbol{x}) = \sum_{k=1}^{N} C_k \lambda^{-\alpha k} \sin(2\pi\lambda^k \boldsymbol{Q}_k \boldsymbol{x} + \Psi_k), \tag{A1}$$

with independent random variables C_k, $\boldsymbol{Q}_k$, and Ψ_k presenting, respectively, normal distribution of zero mean and variance one, uniform distribution on the unit circle, and uniform distribution on $[0,2\pi]$. In the forthcoming λ is set to 1.08 and N to 150. Functions defined by Eq. (A1) mimic the statistical properties of fractional Brownian motion for $|\boldsymbol{\varepsilon}|$'s small compared with the size of the system and above the characteristic cutoff length $l_c \sim \lambda^{-N}$. As seen in Fig. 14(b), the box-counting procedure requires a large statistics to capture the self-similar behavior in the fractal range, squeezed between the under-resolved (large ε's) and regular domains (small ε's).

APPENDIX B: DIRECT EVALUATION OF THE BOX-COUNTING DIMENSION OF SINGULAR VORTICES

Considering an initially straight line intersecting the center of the vortex, the length of the generated spiral is approximated:

$$L = \int_{r_{\text{in}}}^{r_{\text{out}}} \frac{2\pi r}{\delta r} dr \sim \frac{t}{\text{Da}} \left[\left(\frac{t\sqrt{\mathcal{D}t}}{\text{Da}} \right)^{-\beta/(\beta+2)} - \left(\frac{t}{\text{Da}} \right)^{-\beta/(\beta+1)} \right], \tag{B1}$$

with δr, r_{in}, and r_{out} given, respectively, by Eqs. (22), (24), and (28). For $t < \text{Da}^{-2/(\beta-1)} \mathcal{D}^{(\beta+1)/(\beta-1)}$, this length resumes to

$$L_{\mathcal{B}} \propto (\sqrt{\mathcal{D}t})^{-\beta/(\beta+2)} \left(\frac{t}{\text{Da}} \right)^{2/(\beta+2)}, \tag{B2}$$

highlighting the self-similar nature of the spiral with $D_{\mathcal{B}} = (\beta+1)/(\beta+2)$, a cutoff length $\sqrt{\mathcal{D}t}$, and an integral scale r_{out}. The value of $D_{\mathcal{B}}$ as a function of β can be checked in Fig. 15.

[1] J. J. Ou and W. E. Ranz, Chem. Eng. Sci. **38**, 1005 (1983).
[2] F. J. Muzzio and J. M. Ottino, Phys. Rev. A **42**, 5873 (1990).
[3] M. Lindberg and Å. C. Rasmuson, Chem. Eng. Sci. **54**, 483 (1999).
[4] S. Edouard, B. Legras, F. Lefevre, and R. Eymard, Nature (London) **384**, 444 (1996).
[5] D. G. H. Tan, P. H. Haynes, A. R. MacKenzie, and J. A. Pyle, J. Geophys. Res., [Atmos.] **103** (D1), 1585 (1998).
[6] A. Wonhas and J. C. Vassilicos, J. Geophys. Res., [Atmos.] **108** (D11), 4325 (2003).
[7] D. Toussaint and F. Wilczek, J. Chem. Phys. **78**, 2642 (1983).
[8] R. Reigada, F. Sagués, I. M. Sokolov, J. M. Sancho, and A. Blumen, Phys. Rev. E **53**, 3167 (1996).
[9] K. Kang and S. Redner, Phys. Rev. Lett. **52**, 955 (1984).
[10] P. Argyrakis and R. Kopelman, Phys. Rev. A **41**, 2121 (1990).
[11] F. Leyvraz and S. Redner, Phys. Rev. Lett. **66**, 2168 (1991).
[12] G. Zumofen, J. Klafter, and A. Blumen, Phys. Rev. A **44**, 8390 (1991).
[13] F. Leyvraz and S. Redner, Phys. Rev. A **46**, 3132 (1992).
[14] S. B. Yuste, L. Acedo, and K. Lindenberg, Phys. Rev. E **69**, 036126 (2004).
[15] H. Tennekes and J. L. Lumley, *A First Course in Turbulence* (MIT, Cambridge, MA, 1972).
[16] R. T. Pierrehumbert, Chaos **10**, 61 (2000).

[17] A. D. Gilbert, J. Fluid Mech. **193**, 475 (1988).
[18] P. B. Rhines and W. R. Young, J. Fluid Mech. **133**, 133 (1983).
[19] P. Flohr and J. C. Vassilicos, J. Fluid Mech. **348**, 295 (1997).
[20] A. P. Bassom and A. D. Gilbert, J. Fluid Mech. **371**, 109 (1998).
[21] A. P. Bassom and A. D. Gilbert, J. Fluid Mech. **398**, 245 (1999).
[22] P. Meunier and E. Villermaux, J. Fluid Mech. **476**, 213 (2003).
[23] T. S. Lundgren, Chem. Eng. Sci. **40**, 1641 (1985).
[24] F. E. Marble, in *Mixing, Diffusion and Chemical Reaction of Liquids in a Vortex Field*, edited by M. Moreau and P. Turq (Plenum, New York, 1988).
[25] B. M. Cetegen and N. Mohamad, J. Fluid Mech. **249**, 391 (1993).
[26] T. S. Lundgren, Phys. Fluids **25**, 2193 (1982).
[27] H. K. Moffat, S. Kida, and K. Ohkitani, J. Fluid Mech. **259**, 241 (1994).
[28] J. Jiménez, H. K. Moffat, and C. Vasco, J. Fluid Mech. **313**, 209 (1996).
[29] A. Celani, M. Cencini, M. Vergassola, E. Villermaux, and D. Vincenzi, J. Fluid Mech. **523**, 99 (2005).
[30] R. T. Pierrehumbert, Chaos, Solitons Fractals **4**, 1111 (1994).
[31] V. Toussaint, P. Carrière, and F. Raynal, Phys. Fluids **7**, 2587 (1995).
[32] J. T. M. Antonsen, Z. Fan, E. Ott, and E. Garcia-Lopez, Phys. Fluids **8**, 3094 (1996).
[33] E. Balkovsky and A. Fouxon, Phys. Rev. E **60**, 4164 (1999).
[34] Z. Neufeld, C. López, E. Hernández-Garciá, and T. Tél, Phys. Rev. E **61**, 3857 (2000).
[35] G. Károlyi and T. Tél, Phys. Rev. Lett. **95**, 264501 (2005).
[36] S. M. Cox, Physica D **199**, 369 (2004).
[37] P. E. Arratia and J. P. Gollub, Phys. Rev. Lett. **96**, 024501 (2006).
[38] J. Sukhatme and R. T. Pierrehumbert, Phys. Rev. E **66**, 056302 (2002).
[39] D. R. Fereday and P. H. Haynes, Phys. Fluids **16**, 4359 (2004).
[40] J. C. Vassilicos, Philos. Trans. R. Soc. London, Ser. A **360**, 2819 (2002).
[41] H. Chaté and S. R. Cant, Combust. Flame **74**, 1 (1988).
[42] J. C. Vassilicos and N. Nikiforakis, Combust. Flame **109**, 293 (1997).
[43] H. J. Lugt, *Vortex Flow in Nature and Technology* (Wiley, New York, 1983).
[44] P. Saffman, *Vortex Dynamics* (Cambridge University, Cambridge, England, 1992).
[45] W. E. Ranz, AIChE J. **25**, 41 (1979).
[46] J. C. Vassilicos and J. C. R. Hunt, Proc. R. Soc. London, Ser. A **435**, 505 (1991).
[47] A. Wonhas and J. C. Vassilicos, J. Fluid Mech. **442**, 359 (2001).
[48] A. Wonhas and J. C. Vassilicos, Phys. Rev. E **66**, 051205 (2002).
[49] J. C. Vassilicos, in *Topological Aspects of the Dynamics of Fluids and Plasmas* (Kluwer, Dordrecht, 1992), pp. 427–442.
[50] K. Falconer, *Fractal Geometry* (Wiley, New York, 2003).